Network Science **6** (4): 448–468, 2018.
doi:10.1017/nws.2018.14

A study of cascading failures in real and synthetic power grid topologies

RUSSELL SPIEWAK
Yeshiva University, New York, NY, USA
(*e-mail:* russell.spiewak@mail.yu.edu)

SALEH SOLTAN
Princeton University, Princeton, NJ, USA
(*e-mail:* ssoltan@princeton.edu)

YAKIR FORMAN and SERGEY V. BULDYREV
Yeshiva University, New York, NY, USA
(*e-mail:* yakir.forman@mail.yu.edu, buldyrev@yu.edu)

GIL ZUSSMAN
Columbia University, New York, NY, USA
(*e-mail:* gil@ee.columbia.edu)

Abstract

Using the direct current power flow model, we study cascading failures and their spatial and temporal properties in the U.S. Western Interconnection (USWI) power grid. We show that yield (the fraction of demand satisfied after the cascade) has a bimodal distribution typical of a first-order transition. The single line failure leads either to an insignificant power loss or to a cascade which causes a major blackout with yield less than 0.8. The former occurs with high probability if line tolerance α (the ratio of the maximal load a line can carry to its initial load) is greater than 2, while a major blackout occurs with high probability in a broad range of $1 < \alpha < 2$. We also show that major blackouts begin with a latent period (with duration proportional to α) during which few lines overload and yield remains high. The existence of the latent period suggests that intervention during early stages of a cascade can significantly reduce the risk of a major blackout. Finally, we introduce the preferential Degree And Distance Attachment model to generate random networks with similar degree, resistance, and flow distributions to the USWI. Moreover, we show that the Degree And Distance Attachment model behaves similarly to the USWI against failures.

Keywords: *power grids, cascading failures, line failures, synthetic power grids*

1 Introduction

Failure of a transmission line in the power grid leads to a redistribution of the power flows. This redistribution may cause overloads on other lines and their subsequent failures, leading to a major blackout (Bernstein *et al.*, 2014; Pahwa *et al.*, 2014; Buldyrev *et al.*, 2010; Soltan *et al.*, 2014; Hines *et al.*, 2009). These failures may be initiated by natural disasters, such as earthquakes, hurricanes, and solar flares, as well as by terrorist and electromagnetic pulse attacks (U.S FERC *et al.*, 2010). Recent blackouts in the Northeastern United States (US-Canada Power System

Outage Task Force, 2004) and in India (Bakshi *et al.*, 2012) demonstrated that major power outages have a devastating impact on many aspects of modern life. Hence, there is a dire need to study the properties of cascading failures in power grids.

The direct current (DC) power flow model is commonly used in studying failures in power grids (Glover *et al.*, 2012; Soltan *et al.*, 2014; Bienstock, 2011; Carreras *et al.*, 2004; Bienstock & Verma, 2010; Pinar *et al.*, 2010; Carreras *et al.*, 2002; Asztalos *et al.*, 2014; Dobson & Lu, 1992; Bakke *et al.*, 2006). In this paper, we employ a similar power flow model which is equivalent to the flows in a resistor network (De Arcangelis *et al.*, 1985) and follow the cascading failure model of Soltan *et al.* (2014) and Bernstein *et al.* (2014).

It is observed in Carreras *et al.* (2002) that the distribution of blackout occurrences in power grids follows a power law, which is related to the phenomenon of self-organized criticality. Other authors suggest that blackouts follow first-order phase transitions, in which the loss of power is either very small or very large (Zapperi *et al.*, 1997; Pahwa *et al.*, 2014). The goal of this paper is to thoroughly study the properties of cascading failures in power grids and create a realistic model that carries the main features of a real grid. For this reason, we study cascades in the U.S. Western Interconnection (USWI) grid and introduce a synthetic Degree And Distance Attachment (DADA) model.

We show that the characteristics of blackouts are universal. However, the sizes of blackouts are much smaller in the USWI with a realistic design than in an artificial DADA model with a different spatial organization. In particular, we study the dependence of the blackout size and the dynamics of the cascading failures on a set of three parameters that characterize the robustness of the grid: (1) tolerance α, the ratio of the maximum flow a line can carry to its initial load (Kornbluth *et al.*, 2018; Motter & Lai, 2002; Motter, 2004); (2) the minimum flow I_p which any line in the network can carry independent of its initial load; and (3) the amount of flow in the initial failed line compared to the distribution of the flows in the grid (I_u). We characterize I_p and I_u by dimensionless parameters p (called the level of protection) and u (called the significance of initial failure). p and u are the fraction of the lines with flows less than I_p and I_u, respectively.

We show that in a broad range of $1 \leqslant \alpha < 2$, $u \geqslant 0.8$, and $0 < p < 0.95$, large blackouts with yield (the fraction of demand satisfied after the cascade) less than 0.8 may occur with a significant probability both in the USWI and in an artificially constructed DADA grids. Moreover, we find that in this range of parameters the distribution of yield is bimodal, which is consistent with first-order phase transitions. Most importantly, we find that in cascading failures that lead to a large blackout, there is a latent period during which the damage is localized, few lines are failed, and the decrease in yield is insignificant. The existence of this latent period suggests that the majority of blackouts can be effectively stopped by the timely intervention of grid operators. The length of the latent period increases as the tolerance α increases. Another important discovery is that in the event of a large blackout, cascading failures stop when the network breaks into small, disconnected islands.

The rest of the paper is organized as follows. Section 2 describes the power flow and cascading failure models. In Section 3, we study the topological properties of the USWI power grid and its robustness against cascading failures. In Section 4, we

https://doi.org/10.1017/nws.2018.14 Published online by Cambridge University Press

Table 1. Summary of notation.

Notation	Description
n^+	The number of supply nodes
n^-	The number of demand nodes
n^0	The number of transmitting nodes
I_i^+	The current supplied by supply node i
I_i^-	The current demanded by demand node i
R_{ij}	The resistance of the line connecting nodes i and j
V_i	The voltage of node i
I_{ij}	The current traveling through the line connecting nodes i and j
α	The tolerance of the lines
p	The level of protection of the lines
u	The significance of the initial failure

describe the DADA model, and in Section 5 we compare its features to the USWI power grid. Finally, in Section 6, we discuss and summarize the results of our study.

2 Model and definitions

In this section, we describe the power flow and the cascade model in details. Table 1 provides a summary of notations.

2.1 Power flow model

We employ the DC power flow model widely used in the power engineering community. This model is equivalent to the flow equations in resistor networks. In this model, the power flows, reactance values, and phase angles are replaced by currents, resistance values, and the voltages, respectively.

We denote the power grid network by a graph $G = (N, E)$, where N denotes the set of all nodes and E denotes the set of edges. We assume G consists of n^0 transmitting, n^+ supply, and n^- demand nodes. The total number of nodes is $n = n^0 + n^+ + n^-$. Each supply or demand node is specified by the amount of current it supplies ($I_i^+ > 0$) or by the amount of current it demands ($I_i^- > 0$). Due to the law of charge conservation, $\sum I_i^+ = \sum I_i^-$. We denote the set of all neighbors of node i by $N(i)$. $k_i := |N(i)|$ represents the degree of a node i and $\langle k \rangle$ is the average degree of all nodes in the network. Each transmission line connecting nodes i and j is characterized by its resistance R_{ij}, while each node i is characterized by its voltage V_i. The current I_{ij} flowing from node i to node j is

$$I_{ij} = (V_i - V_j)/R_{ij}. \tag{1}$$

Additionally, the sum of all the currents flowing into each node i is equal to the sum of all currents flowing out:

$$\sum_{j \in N(i)} I_{ij} = \delta_i^+ I_i^+ - \delta_i^- I_i^-, \tag{2}$$

where $\delta_i^+ = 1$ or $\delta_i^- = 1$ if a node i is a supply or a demand node, respectively. $\delta_i^+ = \delta_i^- = 0$ otherwise.

https://doi.org/10.1017/nws.2018.14 Published online by Cambridge University Press

2.2 Cascading failures model

Once the system (1)–(2) is solved, we find the currents in all transmitting lines I_{ij} and define their maximum capacities I_{ij}^* using the following two rules: (i) we define I_p as the standard capacity of the lines. It is computed such that a fraction p of the lines initially have currents below I_p. We refer to p as the *level of protection*. (ii) For each line, we define its individual capacity $\alpha|I_{ij}|$, where $\alpha \geqslant 1$ is the *tolerance* (i.e., the factor of safety). We assume α to be the same for every transmission line in the grid. Using these rules,

$$I_{ij}^* \equiv \max(I_p, \alpha|I_{ij}|). \tag{3}$$

If a current in line $\{i, j\}$ exceeds I_{ij}^*, it fails.

The larger p and α are, the better the grid is protected against overloads. The standard capacity I_p is to ensure that lines that do not carry a significant current have a reasonable capacity. In this paper, we use $p = 0.9$ and vary α as the main parameter of grid resilience, most of the time.

To initiate a cascading failure, we randomly select and remove a single line which current $|I_{ij}|$ belongs to the interval $[I_{u-\Delta u}, I_u]$, where the fraction $u - \Delta u$ of lines operate below $I_{u-\Delta u}$ and the fraction u of lines operate below I_u. The parameter u specifies the significance of the lines which are targeted for the initial failure. We refer to u as the *significance of the initial failure*. For example, $u = 1.0$ and $\Delta u = 0.1$ means that the line which is initially failed, is selected from the top 10% of lines ranked according to their initial current.

Removing a line can lead to disintegration of the grid into two disconnected components, which we call clusters. Obviously, the supply and demand in each cluster should be equalized to retain charge conservation. Thus, for each cluster C_j, we compute $\sum_{i\in C_j} I_i^+$ and $\sum_{i\in C_j} I_i^-$. If in a cluster $\sum_{i\in C_j} I_i^+ > \sum_{i\in C_j} I_i^-$, we multiply the current of each supply node in C_j by $\frac{\sum_{i\in C_j} I_i^-}{\sum_{i\in C_j} I_i^+} < 1$; if $\sum_{i\in C_j} I_i^- > \sum_{i\in C_j} I_i^+$, we multiply the current of each demand node in C_j by $\frac{\sum_{i\in C_j} I_i^+}{\sum_{i\in C_j} I_i^-} < 1$ to obtain new supply/demand values $I_i^{+(1)}$ and $I_i^{-(1)}$. We define $I_1 = \sum_i I_i^{+(1)} = \sum_i I_i^{-(1)}$ as the total supplied current at the end of the first step of the cascade. Then, we solve Equations (1) and (2) again to compute new new currents $I_{ij}^{(1)}$. At the second time step of the cascade, we remove all lines for which the new current $|I_{ij}^{(1)}|$ exceeds its maximum capacity I_{ij}^*. If no overloads occur, the cascade stops. If there are new failures, we repeat the supply/demand equalization process, modify the system of equations (1)–(2), and compute the new currents $I_{ij}^{(2)}$. We repeat this process recurrently until at a certain time step t of the cascade no lines fail. We call this time step, the final step of the cascade.

2.3 Metrics

We define here all the metrics used in this paper to characterize the severity of a cascade.

Cascade Duration, f: the number of time steps until the cascade stops.

https://doi.org/10.1017/nws.2018.14 Published online by Cambridge University Press

Number of Active Lines, L: the number of transmission lines in the grid that have not failed by the end of the cascade.

Yield, $Y(t)$: $\frac{I_t}{I_0}$, the ratio between the total demand at time step $t(I_t)$ and the original demand (I_0). For $t = f$, we simply denote yield by Y.

Local Yield, $Y(t, h)$:

$$Y(t,h) = \frac{\sum_{i \in H(h)} I_i^{-(t)}}{\sum_{i \in H(h)} I_i^{-}} \tag{4}$$

where $H(h)$ is the subset of demand nodes a given hop distance h from the failed line.

Blackout Radius of Gyration, $r_B(t)$: a quantitative measure of the blackout's geometric dimension as a function of the cascade time step t,

$$r_B(t)^2 = \frac{\left\langle \sum_{i \in B(t)} h_i^2 I_i^{-(t)} \right\rangle}{\left\langle \sum_{i \in B(t)} I_i^{-} \right\rangle} \tag{5}$$

where the summation is made over the set $B(t)$ of totally disconnected demand nodes which do not receive any current at the tth time step of the cascade. $< . >$ denotes the average over all the cascade simulations.

3 The topological properties of the USWI and its robustness against cascades

In this section, we study the properties of the USWI network obtained from the Platts Geographic Information System (Platts, 2009). This dataset includes approximate information about transmission lines based on their lengths, supplies based on power plants' capacities, and demands based on the population at each location (Bernstein *et al.*, 2014). In the next section, we provide the DADA model to generate synthetic power grids. Figures in this section also show the properties of the DADA model that we get back to in the next section.

3.1 Topological properties

The USWI power grid contains 8,050 transmitting nodes, 1,197 supply nodes, 3,888 demand nodes, and 17,544 transmission lines. To avoid exposing possible vulnerabilities of the actual USWI, our dataset does not include the geographic coordinates of the nodes. It does however, include the length of each line r_{ij} connecting nodes i and j. We define the resistances of the lines to be proportional to their lengths $R_{ij} = \rho r_{ij}$, where ρ is a constant.

3.1.1 Degree distribution

The degree distribution of the nodes in the USWI is characterized by a fat-tail distribution (Figure 1(a)), which can be approximated by a power law $P(k) \approx k^{-3}$ with an exponential cut-off. The degree distribution of transmitting nodes, supply nodes, and demand nodes are quite similar to each other. The average degree $\langle k \rangle$ of

https://doi.org/10.1017/nws.2018.14 Published online by Cambridge University Press

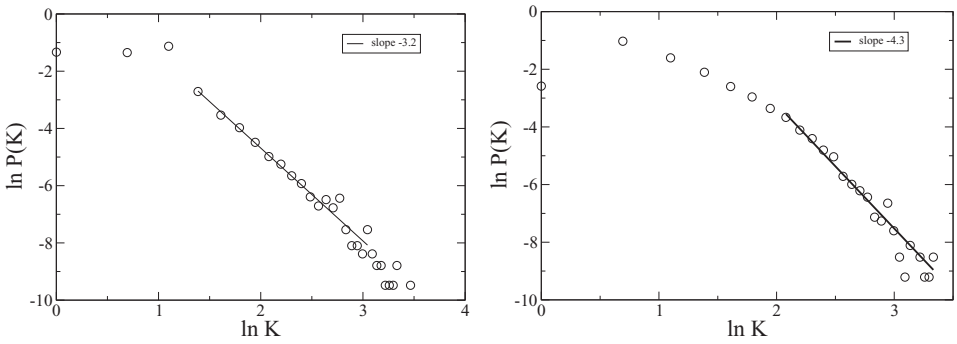

(a) USWI (b) DADA

Fig. 1. Degree distributions of the nodes in (a) the USWI power grid, and (b) the DADA model for $\mu = 6$, $\ell = 1.5$.

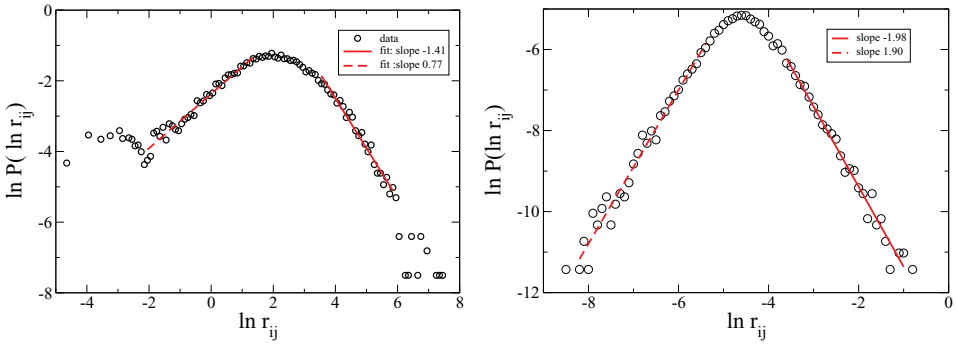

(a) USWI (b) DADA

Fig. 2. Length distribution of the lines, which are the same as the resistance values, in (a) the USWI power grid, and (b) the DADA with $\mu = 6$, $\ell = 1.5$. (Color online)

the nodes in the USWI is 2.67. For the supply nodes, it is slightly larger 2.88 and for the demand nodes, it is slightly smaller 2.61.

3.1.2 Length distribution of the lines

The length distribution of the lines in the USWI has an approximately lognormal shape with power law tails. Figure 2(a) shows $\ln P(\ln r_{ij})$, the logarithm of the probability density function (PDF) of $\ln r_{ij}$. For the lognormal distribution, the curve would be a perfect parabola. Instead, we see that both tails of the distribution can be well approximated by straight lines with slope $v_- = 0.77$ for the left tail and slope $v_+ = -1.44$ for the right tail. This means that the PDF of r_{ij} can be approximated by power laws $P(r) \approx r^{v_- - 1}$ for $r \to 0$ and $P(r) \approx r^{v_+ - 1}$ for $r \to \infty$.

3.2 Cascade properties

The results provided in this subsection are for 100 trials for each set of p, u, α. In this subsection, $\Delta u = 0.1$.

https://doi.org/10.1017/nws.2018.14 Published online by Cambridge University Press

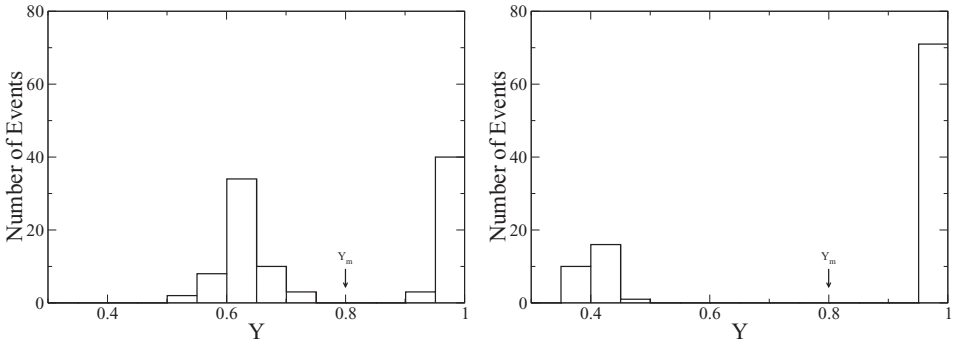

Fig. 3. Distribution of yield for $\alpha = 1.6$, $p = 0.9$, and $u = 1.0$ in (a) USWI and (b) DADA.

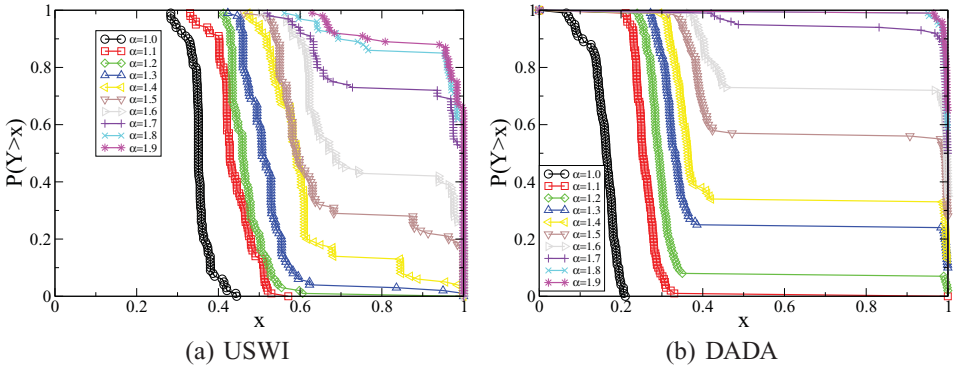

Fig. 4. Cumulative distribution of the yield for $p = 0.9$, $u = 1.0$ and various values of α for (a) the USWI model, and (b) the DADA model with $\mu = 6$, $\ell = 1.5$. The large gap in the distributions is a feature of the abrupt first-order transition. (Color online)

3.2.1 *Bimodality of the yield distribution*

The interesting feature of the yield histogram as can be seen in Figure 3(a), is its bimodality. One can clearly see the bimodality of the distribution with two peaks for high yield 0.975 and low yield 0.625, with practically no yields between 0.75 and 0.9 for the USWI. This can be detected by a plateau in the cumulative yield distribution (Figure 4(a)). The bimodality of the yield distribution is present in a large region of the parameter space (α, p, u), characterized by relatively small $\alpha < 2$, practically all $p \leqslant 0.95$, and relatively large $u > 0.8$. One can see (Figure 4(a)) that the distribution of yield clearly remains bimodal for $\alpha < 2$ in the USWI model.

3.2.2 *Risk of large blackouts*

Cascades can be characterized by two important parameters of the outcome: (i) the probability of a large blackout $P(Y < 0.8)$, which we call the risk of a large

https://doi.org/10.1017/nws.2018.14 Published online by Cambridge University Press

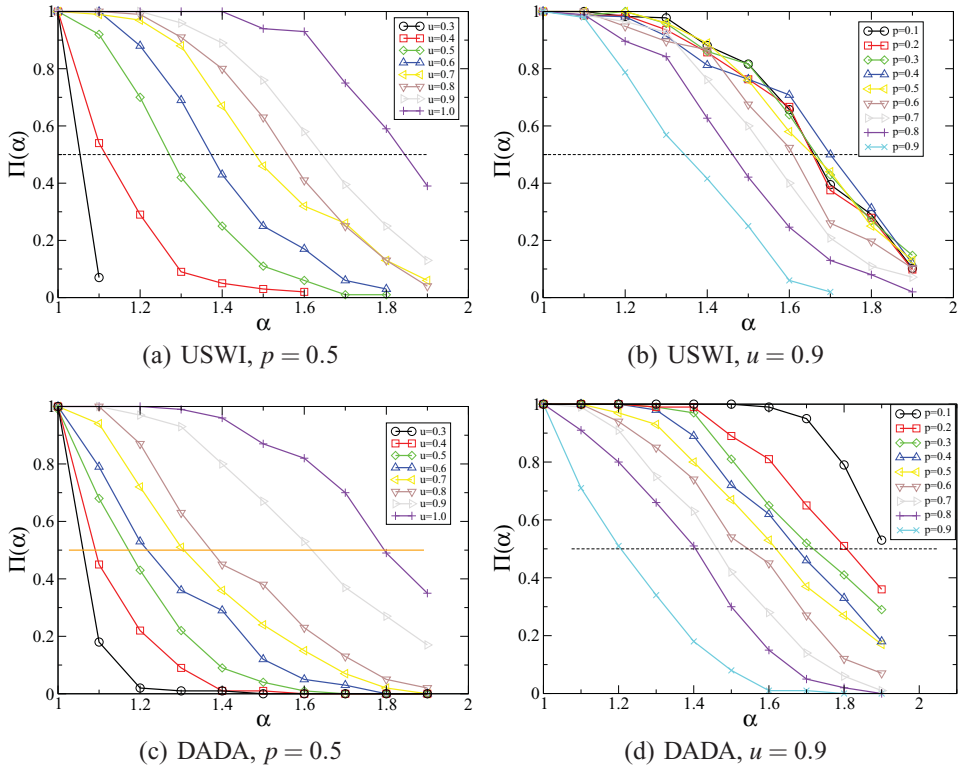

(a) USWI, $p = 0.5$ (b) USWI, $u = 0.9$

(c) DADA, $p = 0.5$ (d) DADA, $u = 0.9$

Fig. 5. Probability of large blackout $P(Y < 0.8)$, or risk $\Pi(\alpha)$, as function of α in (a) USWI model for different values of u and $p = 0.5$, (b) USWI model for different values of p and $u = 0.9$, (c) DADA model for different values of u and $p = 0.5$, and (d) DADA model for different values of p and $u = 0.9$. (Color online)

blackout $\Pi(\alpha)$, and (ii) the average blackout yield $\langle Y \rangle$, for the cases result in a large blackout.

Figure 5(a) and (b) shows how the risk of large blackouts $\Pi(\alpha)$ decreases as α increases for different values of u and p. We find that for different values of u and p, the shapes of the curves $\Pi(\alpha)$ remain approximately constant, but the curves significantly shift in a horizontal direction. This means that the curves $\Pi(\alpha)$ can be well approximated by $\Pi(\alpha - \alpha_0(u, p))$. The function $\alpha_0(u, p)$ can be defined by solving the equation $\Pi(\alpha_0(u, p)) = \frac{1}{2}$ with respect to $\alpha_0(u, p)$. One can see that $\alpha_0(u, 0.5)$ is an approximately linear function of u, which increases with u (Figure 6(a)). This means that for protection against failure in lines carrying high currents, a higher tolerance is needed. In other words, the same effect can be achieved either by protecting a certain fraction of the most significant lines from spontaneous failure, or by increasing the tolerance of all the lines by some quantity (Figure 6(a)).

The dependence of the risk on p is weaker than on u, especially for $p \leqslant 0.5$ (Figure 6(b)). An increase in p has practically no effect on the robustness of the grid. The increase in p achieves a significant effect on the risk of large blackouts only when p approaches 0.9.

https://doi.org/10.1017/nws.2018.14 Published online by Cambridge University Press

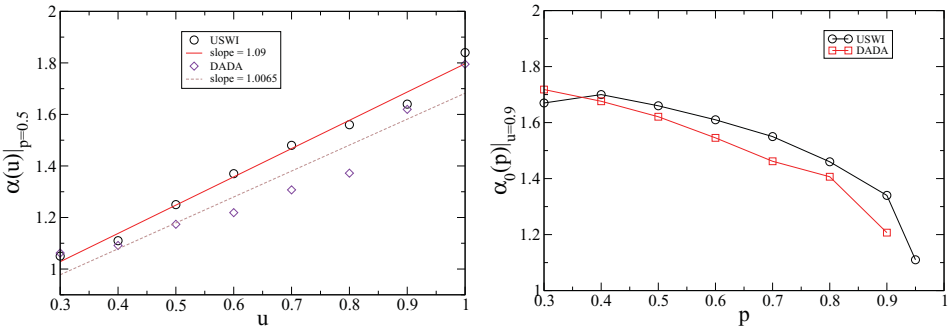

(a) $p = 0.5$ (b) $u = 0.9$

Fig. 6. Behavior of $\alpha_0(u, p)$ (a) as function of u at constant $p = 0.5$, and (b) as function of p at constant $u = 0.9$. (Color online)

3.2.3 *Characteristics of large blackouts*

Large blackouts can be characterized by their average yield $\langle Y \rangle$, average fraction of surviving lines $\langle L \rangle$, and the average fraction of nodes in the largest connected component of the grid $\langle G \rangle$. These metrics only weakly depend on u, but are strongly increasing functions of α (Figure 7(a)). The independence of the characteristics of large blackouts on u stems from the fact that the properties of large blackouts, if they occur, do not depend on a particular line to initiate the failure. The risk of large blackouts depends on u, but the average parameters of large blackouts do not.

The dependence of these metrics on p is more complex (Figure 7(b)). While the yield $\langle Y \rangle$ starts to increase only for $p > 0.7$, the number of survived lines $\langle L \rangle$ significantly increases with p even for small p. This is not surprising since p is the level of protection of the lines, and fewer lines fail if more lines are protected. As p approaches 1, the dependence of $\langle L \rangle$ on α becomes very weak. The explanation of this fact is based on the notion that $\langle L \rangle$ is computed only for the case of *large* blackouts. For a large blackout to occur, a significant fraction of lines must fail, sufficient to disconnect a large fraction of demand nodes. On the other hand, as α increases, the risk of a large blackout goes to zero, so the average fraction of lines surviving for all the cascades (large and small) approaches 1.

Another important observation from Figure 7(b) is the small dependence of $\langle G \rangle$ on the parameters α, p, and u, as opposed to $\langle L \rangle$. Hence, by removing a small fraction of the lines (20%), the grid disintegrates into many small clusters, each less than 20% of the total size. Indeed, percolation theory predicts that close to the percolation threshold, it is sufficient to delete an infinitesimally small fraction of the so called "red" bonds to divide the network into a set of small disconnected components (Coniglio, 1981).

3.2.4 *Latent period of the cascade*

The cascading failures that do not result in large blackouts ($Y > 0.8$) are usually short ($f < 8$) (Figure 8(a) and (b)). In contrast, the duration of cascades resulting in large blackouts ($Y \leqslant 0.8$) increases with α, reaching values of order 40 for large α.

https://doi.org/10.1017/nws.2018.14 Published online by Cambridge University Press

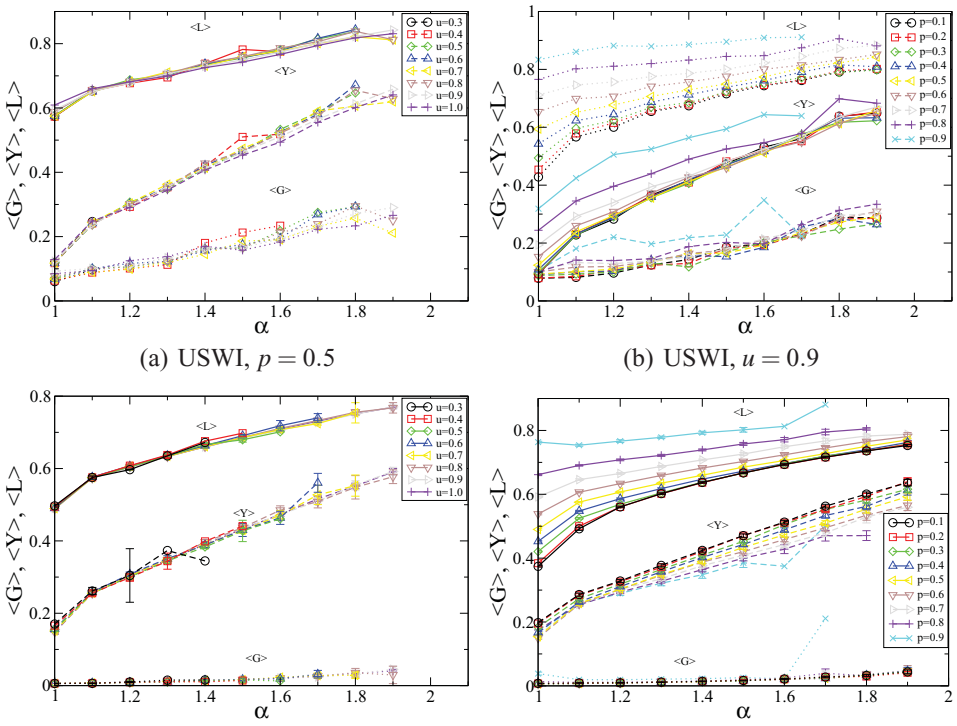

(a) USWI, $p = 0.5$ (b) USWI, $u = 0.9$

(c) DADA, $p = 0.5$ (d) DADA, $u = 0.9$

Fig. 7. Behavior of the yield $\langle Y \rangle$, the fraction of nodes in the largest connected component $\langle G \rangle$, and the fraction of survived lines $\langle L \rangle$ averaged over cascades resulted in large blackouts ($y < 0.8$) as a function of α for different u and a fixed value of $p = 0.5$ in (a) USWI model, and (c) DADA model. The behavior for different p at fixed $u = 0.9$ in (b) USWI model, and (d) DADA model. (Color online)

This means that for large tolerances, it takes much longer for the cascade to spread over a large area, since at each time step only a few lines overload and fail.

In the cascades resulting in large blackouts, yield $Y(t)$ decreases with time in a non-trivial way (Figure 9(a)). During the first few time steps of the cascades, the yield does not significantly decrease since the current can successfully redistribute over the remaining lines without disconnection of the demand nodes. This period, in which the cascade is still localized and a blackout has not yet occurred, can be called the *latent period of the cascade*, t_l. The recognition of this latent period is important since it is a period in which a cascade is beginning to spread but has not yet grown uncontrollable. In the latent period, it may still be possible to intervene and redistribute current flow to stop the cascade before it becomes a large blackout.

We define the duration of this latent period of the cascade as the time step at which the yield drops below 0.95. At approximately this time step, the yield starts to rapidly decrease and then, toward the end of the cascade, stabilizes again. The shape of this function is characteristic of an abrupt first-order transition observed in simpler models of network failure (Buldyrev *et al.*, 2010; Motter, 2004). Remarkably, the duration of the latent period is a linear function of tolerance (Figure 9(b)).

https://doi.org/10.1017/nws.2018.14 Published online by Cambridge University Press

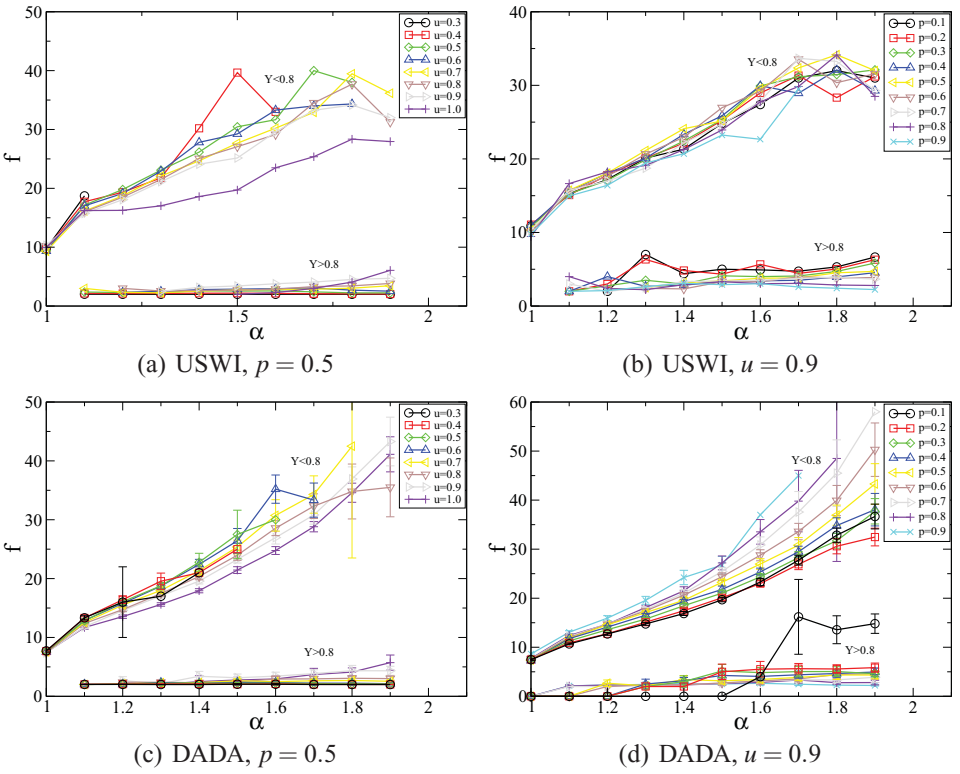

(a) USWI, $p = 0.5$ (b) USWI, $u = 0.9$

(c) DADA, $p = 0.5$ (d) DADA, $u = 0.9$

Fig. 8. Dependence of the average duration of the cascade on tolerance α for different u at $p = 0.5$ in (a) USWI model, and (c) DADA model. The dependence for different p at $u = 0.9$ in (b) USWI model, and (d) DADA model. (Color online)

3.2.5 *Cascade spatial evolution*

To observe the spatial evolution of a cascade, we group the grid's demand nodes into bins based on their "hop distance" from the original failed line. In each bin, we compute the local yield $Y(t,h)$. We average the local yield $Y(t,h)$ for cascades resulting in large blackouts (Figure 10(a)). The yield in each bin at the end of cascades resulting in large blackouts is almost independent of the distance from the initially failed line. While at the beginning of the cascade, the blackout is localized near the initially failed line, eventually the blackout spreads uniformly over the entire system. Delocalization occurs at the end of the latent period of the cascade. This can be clearly seen from the behavior of the blackout profiles, which start to rapidly drop down for large distances only at intermediate time steps of the cascade.

To give a more quantitative measure of the blackout spread, we use the "blackout radius of gyration" ($r_B(t)$) metric defined in Section 2.3. Figure 11 shows the behavior of $r_B(t)^2$ versus the cascade time step t for the cascades which result in insignificant failures (Figure 11(a)) and large blackouts (Figure 11(b)). We observe the same phenomena—initially $r_B(t)^2$ grows slowly in all the cascades. However, while in cascades resulting in insignificant consequent failures the cascade stops during the latent period, in ones resulting in large blackouts the cascade rapidly spreads over a large area. The cascade spreads more quickly for small α than for large α.

https://doi.org/10.1017/nws.2018.14 Published online by Cambridge University Press

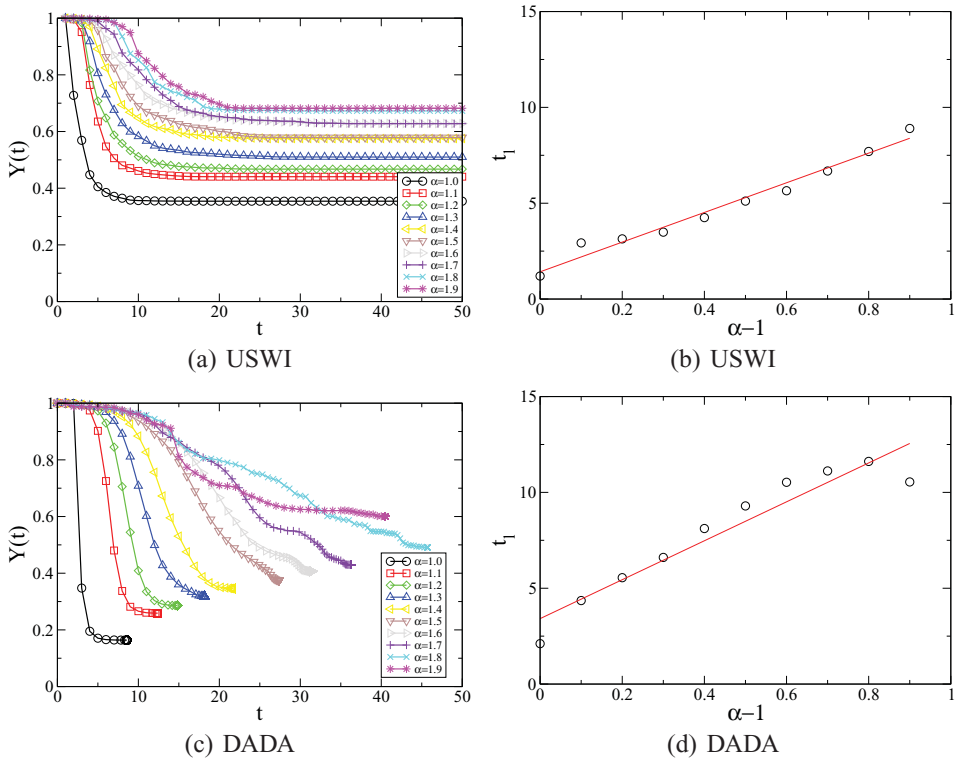

Fig. 9. Yield as a function of the cascade time steps for the cascades resulting in large blackouts in (a) the USWI model, and (c) the DADA model. The latent period as a function of the tolerance α in (b) the USWI model, and (d) the DADA model. In both USWI and DADA models, $u = 1.0$, $p = 0.9$. (Color online)

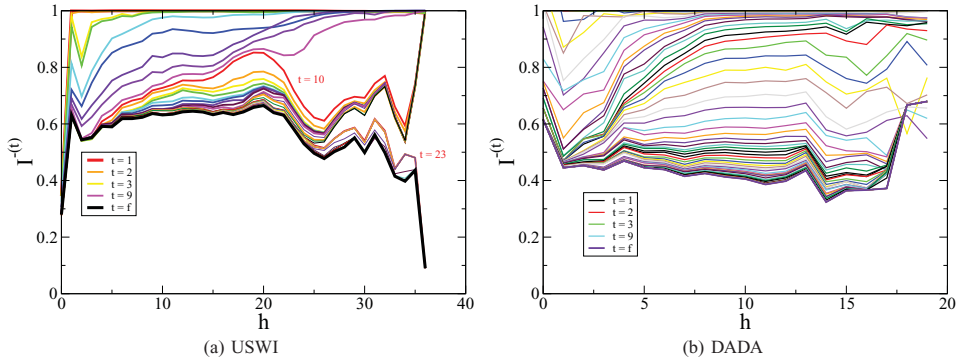

Fig. 10. The fraction of current reaching demand nodes as a function of hop distance in cascades resulting in large blackouts in different cascade time steps, with $p = 0.9$ and $\alpha = 1.6$ in (a) the USWI, and (b) in the DADA model. (Color online)

4 DADA model

In the previous section, we found that cascading failures in the USWI model have characteristic features of a first-order transition: the bimodal distribution of yield

https://doi.org/10.1017/nws.2018.14 Published online by Cambridge University Press

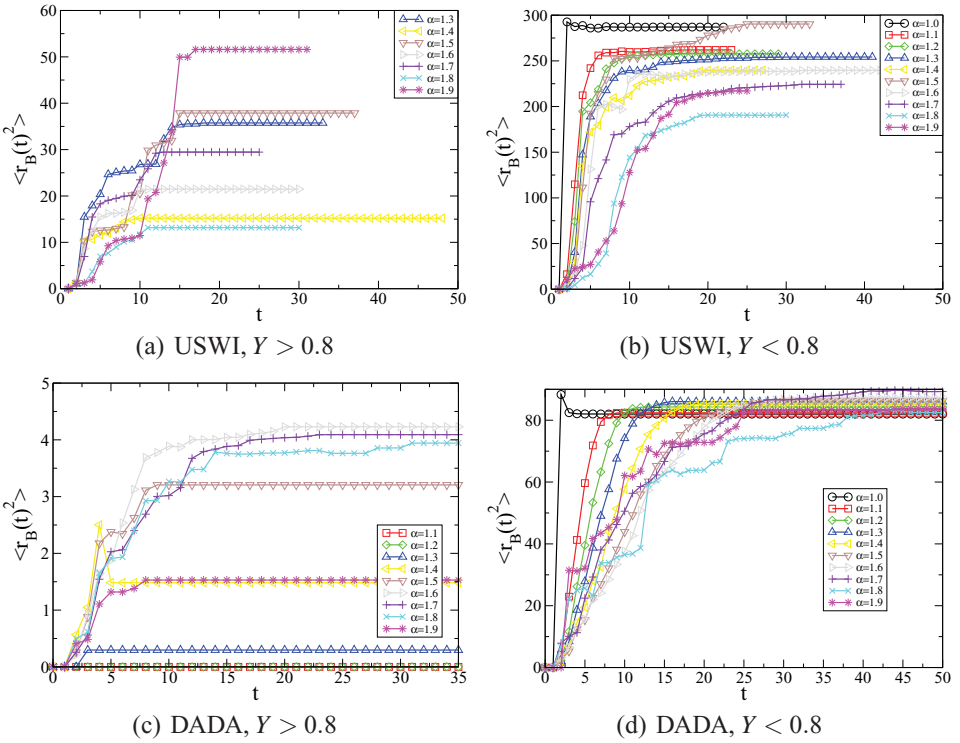

(a) USWI, $Y > 0.8$ (b) USWI, $Y < 0.8$

(c) DADA, $Y > 0.8$ (d) DADA, $Y < 0.8$

Fig. 11. The averaged behavior of the radius of gyration of the cascading failures in small blackouts $Y > 0.80$ in (a) the USWI model and (c) the DADA model, and large blackouts with $Y < 0.80$ in (b) the USWI model and (d) the DADA model. (Color online)

and the latent period during which the damage to the network is insignificant. It is important to investigate whether these features are due to particular characteristics of the USWI design, or whether they are universal features of a much broader class of networks. Moreover, the data on real grids are limited and therefore it is important to develop algorithms for generating synthetic grids resembling real grids topologies.

The two basic features of USWI that we like to reproduce are the degree distribution and the length distribution of the lines. The degree distribution of the USWI discussed in Section 3 is in agreement with the Barabási–Albert preferential attachment model (Albert & Barabási, 2002; Barabási & Albert, 1999). Accordingly, we use the Barabási–Albert model as the basis of the DADA model. In the original Barabási–Albert model, a newly created node is attached to an existing node with a probability proportional to its degree. However, for power grids embedded in two-dimensional space, the length distribution of the lines, resulting from the degree preferential attachment, would not decrease with length. Therefore, in order to create a grid with a decreasing length distribution, one must introduce a penalty for attaching to a distant node. Thus, we employ here the DADA model with a distance penalty, similar to Xulvi-Brunet & Sokolov (2002) and Manna & Sen (2002). This

https://doi.org/10.1017/nws.2018.14 Published online by Cambridge University Press

method produces degree and length distributions similar to those of the USWI (see Section 3.1).

4.1 Construction of the DADA model

4.1.1 Construct the network

The DADA model randomly generates nodes $j = 1, 2, \ldots, n$ one by one on a plane with a uniform density. It connects each new node j to an existing node i based on i's degree and distance with probability $\mathrm{P}(\{i,j\}) \propto \frac{k_i}{r_{ij}{}^{\mu}}$, where k_i is the present degree of node i and r_{ij} is the distance between nodes i and j. This rule mimics the way real networks are evolved. A real network such as the USWI is not planned all at once; rather, new stations are added to the grid as necessity dictates. The probability of connection $\mathrm{P}(\{i,j\}) \propto \frac{k_i}{r_{ij}{}^{\mu}}$ is assumed to be proportional to k_i, since connections to nodes of high degree are more reliable, but also inversely proportional to a power of r_{ij}, since construction of long transmission lines costs more. The distance penalty μ is a factor which seeks to optimize the balance between reliability and cost.

It is shown in Xulvi-Brunet & Sokolov (2002) and Manna & Sen (2002) that for $\mu < 1$, the degree distribution of the resulted graph is a power law $P(k) \approx k^{-3}$, while for $\mu > 1$, it becomes a stretched exponential (Clauset *et al.*, 2009). However, the fat tail of the stretched exponential can be approximated by a power law $P(k) \approx k^{-\gamma}$ with an exponent $\gamma > 3$ (Figure 1(b)). It is also shown in Manna & Sen (2002) that the length distribution of the lines is $P(r_{ij}) \approx r_{ij}$ as $r_{ij} \to 0$, and for large μ, $P(r_{ij}) \approx r_{ij}^{-3}$ as $r_{ij} \to \infty$. The functional form of $P(r_{ij})$ for the DADA and USWI models are similar, but the exponents are different. As mentioned in Section 3.1.2 regarding the USWI model, these asymptotic behaviors correspond to the slopes $v_- = 2$ and $v_+ = -2$ of the logarithmic distribution $P(\ln(r_{ij}))$ observed in the DADA model (Figure 2(b)), while for the USWI model these values are $v_- = 0.77$ and $v_+ = -1.43$. In our simulations, we select $\mu = 6$. For this choice of μ, the degree distribution exponent $\gamma \approx 4.3$, while $-v_+ = 2$. The corresponding values in the USWI model are smaller. Both γ and $-v_+$ can be decreased by decreasing μ, so that the degree and length distributions of the DADA model would be closer to those of the USWI. However, by doing so, our results on the distribution of currents in the DADA model and the properties of the cascading failures do not change significantly, indicating that the observed features of the cascades are quite universal. The discrepancy in v_- for the DADA and USWI is related to the fact that in the DADA model the nodes are spread on the plane with a uniform density, while in the USWI model the density of nodes is related to the population density which has fractal-like features.

Our goal is to create a grid with a given number of lines, l. Therefore, when each new node is created, we connect it on average to $\bar{\ell} = \frac{l}{n} = \frac{\langle k \rangle}{2}$ pre-existing nodes. Since $\bar{\ell}$ is a real number, we pre-assign to each node i an integer ℓ_i, the number of lines by which it will be connected to the previously generated nodes. We randomly select $l - n\lfloor\bar{\ell}\rfloor < n$ nodes, where $\lfloor\bar{\ell}\rfloor$ is the integer part of $\bar{\ell}$. For these nodes, we choose $\ell_i = \lfloor\bar{\ell}\rfloor + 1$. For the rest of the nodes, we choose $\ell_i = \lfloor\bar{\ell}\rfloor$. For each new node j, we attempt to create ℓ_j lines with the previously existing nodes. If $j \leqslant \ell_j$, then we connect j to all pre-existing nodes, as we cannot create ℓ_j lines without

https://doi.org/10.1017/nws.2018.14 Published online by Cambridge University Press

duplicating lines. If $j \geqslant \ell_j$, there are more existing nodes than ℓ_j and we create lines according to the rule described above (with probability proportion to the distance and degree). In the end, a total of almost $n\bar{\ell} = l$ lines are created.

For the USWI network $\bar{\ell} = \langle k \rangle / 2 \approx 1.5$, so for the DADA model, we choose $\bar{\ell} = 1.5$ (more accurate values of $\bar{\ell}$ do not significantly affect our results). Averaging over 100 different grids, our DADA model has slightly higher average degree of 2.84. More accurate values of $\bar{\ell}$ do not significantly change the cascading properties of the DADA model.

As in the USWI model, we assume that in the DADA model $R_{ij} = \rho r_{ij}$, where ρ is resistivity, which is constant for all the lines in the system.

4.1.2 Generate supply and demand

We randomly assign n^+ supply nodes and (different) n^- demand nodes. We select $n = 13,135$, $n^- = 3,888$, and $n^+ = 1,197$ to match the USWI. We assign the supply and demand nodes independent of the nodes' degree. Thus, the average degrees of the supply and demand nodes are the same as the average degree of the DADA model. Since the supplies and demands of the USWI have an approximately lognormal distribution (see Figure 12), we generate currents of supplies and demands in the DADA model following a modified lognormal distribution:

$$I_i^+ = e^{v_i \sigma^+ + m^+ \ln k_i}, \tag{6}$$

for supplies and

$$I_i^- = e^{v_i \sigma^- + m^- \ln k_i}, \tag{7}$$

for demands, where v_i is randomly generated according to a standard normal distribution, $\sigma^\pm$ is a standard deviation, and $m^\pm$ is a parameter which creates a correlation between the node's current and its degree.

Furthermore, since it is unrealistic to have nodes with very high supply and demand vales, we introduce a cut-off $a^\pm \sigma^\pm$, where $a^\pm$ is a parameter of the model such that we accept only $I_i^\pm \leqslant e^{a^\pm \sigma^\pm}$. Thus, the supply and demand of each node is

$$I_i^\pm = \min\left(e^{v_i \sigma^\pm + m^\pm \ln k_i}, e^{a^\pm \sigma^\pm}\right). \tag{8}$$

This cut-off corresponds to the sharp drops of the right tails of the supply and demand distributions in the USWI (Figure 12).

To best match the USWI data, we let the values of $m^\pm$ be the slopes of the regression lines of the log–log scatter plots which plot the average supply or demand versus the degree of corresponding nodes. We then select values of σ and a so that the distributions simulated for the DADA model best match the USWI distributions (Figure 12). We obtain $\sigma^+ = 2.0$, $m^+ = 0.38924$, $a^+ = 1.6$, $\sigma^- = 1.8$, $m^- = 0.62826$, and $a^- = 1.2$.

5 Comparison of the USWI and DADA model

Here, we compare the main properties of the USWI and the DADA model. We also discuss reasons for the differences observed. The cumulative distribution of currents in the DADA model closely follows the exponential distribution of currents in the

https://doi.org/10.1017/nws.2018.14 Published online by Cambridge University Press

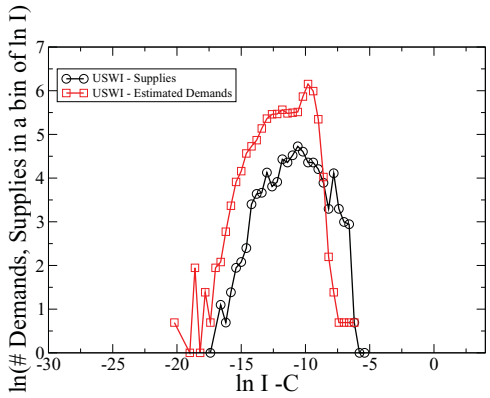

Fig. 12. Distribution of the supply and demand currents in the USWI power grid. Currents are portrayed in arbitrary units. (Color online)

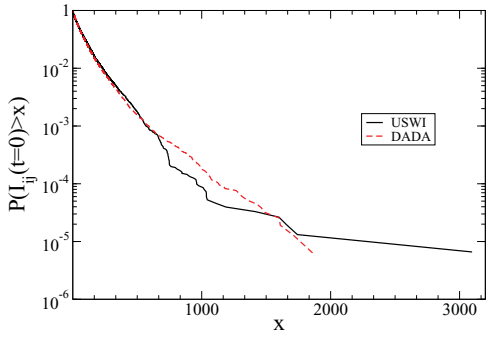

Fig. 13. Cumulative distribution of currents for the USWI model power grid and DADA model with $\mu = 6$ and $\ell = 1.5$. (Currents are measured in arbitrary units.) (Color online)

USWI grid (Figure 13). This is important because the ratio of currents in the two models corresponding to the same significance of lines parameters u is approximately equal.

5.1 Yield

The distribution of the yield Y in the DADA model is also bimodal for approximately the same set of parameters α, u, and p as in the USWI model, but the gap between the two modes (low and high yield) is significantly wider in the DADA model than in the USWI model (Figure 4).

Figure 4 shows the yield distributions of the USWI and DADA model for $u = 1$ and $p = 0.9$ for several values of $1 \leqslant \alpha < 2$. In both networks, the cascade results in a large blackout ($Y < 0.8$) for small values of α, and results in an insignificant consequent failures ($Y > 0.8$) for large values of α. But for the DADA model, chances of large blackout (risk) are smaller for the same set of parameters than in the USWI model. For example, the DADA model can still survive with a small

https://doi.org/10.1017/nws.2018.14 Published online by Cambridge University Press

probability for $\alpha = 1.2$, but the USWI always collapses for $\alpha < 1.3$. Conversely, we do not observe any large blackouts in the DADA model for $\alpha > 1.7$, while a failure in the USWI can still cause large blackouts even for $\alpha = 1.9$. Thus, even though in the event of a large blackout the average yield in the USWI is greater than in the DADA model (and thus, in this sense, the DADA model is more vulnerable than the USWI), the risk of large blackouts is greater in the USWI than in the DADA model for the same set of parameters.

These differences may be related to the fractal structure of the USWI, in which densely populated areas with lot of demand and supply nodes are separated by large patches of empty land over which few long transmission lines are built, whereas the DADA model has constant density of nodes. Thus, it is less likely that the cascade spreads over the entire grid in the USWI. However, a higher tolerance is needed to prevent large blackouts in the USWI than in the DADA model.

Qualitatively, the behaviors of the metrics $\langle Y \rangle$, $\langle L \rangle$, and $\langle G \rangle$ are similar in the USWI model and in the DADA model, but in the DADA model the survival quantities are always smaller for the same α, u, and p. This indicates that the artificial DADA model is more vulnerable than the USWI (Figures 5–7). The values of $\langle G \rangle$ in the DADA model are very small, indicating that in the event of a large blackout the DADA network disintegrates into very small connected components, each constituting about 1% of the nodes of the grid. In the USWI grid, the average largest component is larger, because USWI grid consists of several dense areas connected by few long lines. The overload of these long lines breaks the USWI grid into relatively large disconnected components, preventing the cascade from further spreading.

5.2 Cascade temporal dynamics

The spatial and temporal behaviors of the cascades in the DADA model closely follow the behaviors in the USWI model (Figures 8–11). $r_B(t)^2$ in the DADA model is much smaller than in the USWI model due to the different structures of the models and difference in diameters of the networks. The longest distance (in terms of number of hops) between any two nodes (i.e., diameter of the network) in the DADA model is ≈ 16, while in the USWI model it is ≈ 41. In both models, we see that the cascade spreads more quickly for a small α than for a large α. However, the first-order all-or-nothing nature of the cascades, characterized by a latent period during which the blackout is small and localized followed by a fast blackout spread over a large area, is common in both models.

5.3 Cascade spatial evolution

The advantage of the DADA model is that we know the exact coordinates of the nodes and thus we can illustrate the spatial and temporal evolution of a cascade as a sequence of snapshots on the plane. Figure 14 shows spatial snapshots of the cascading failures taken at different time steps for the DADA model with parameters $\alpha = 1.8$ and $p = 0.4$. The color of each line indicates the time step of the cascade at which the line is failed. One can see that during the first three time steps of the cascade (red lines) the area of line failures is small and localized near the initial

https://doi.org/10.1017/nws.2018.14 Published online by Cambridge University Press

Fig. 14. Cascade propagation for $\alpha = 1.8$, $p = 0.4$, $u = 1$ in the DADA model with 13,135 nodes, $\ell = 1.5$, $\mu = 6$. Lines that failed at different time steps of the cascade are shown with different colors. The initial line randomly selected to fail due to spontaneous failure or attack is depicted at the center of the grid and is surrounded by a gray circle. (Color online)

failure. The cascade starts to spread during time steps 4–8 (orange and yellow–green), but the area of line failures is still localized. At time step 10, the cascade quickly spreads to very distant parts of the system (green). The blue and violet lines are the final time steps of the cascade. Thus, the figure also illustrates the latent period of the cascade during which the distressed area is small and localized.

6 Conclusion

In this paper, we thoroughly studied the properties of cascading failures in power grids. We showed that the cascading failures in power grids have features of all-or-nothing transition, just like in a broad spectrum of more primitive models such as the Motter model (Motter & Lai, 2002; Motter, 2004). In the Motter model, instead of currents, the betweenness of each node in a graph is computed and the maximum load of each node is defined as its original betweenness multiplied by the tolerance. Then, a random node is taken out as an initial failure, and the new betweenness of each node is calculated. If the new betweenness of a node exceeds its maximum load, this node is taken out and the entire process is repeated. The yield in the

https://doi.org/10.1017/nws.2018.14 Published online by Cambridge University Press

Motter model is defined as the fraction of survived nodes at the end of the cascade. The distribution of the yield in the Motter model is bimodal for a large range of tolerances. Similarly, in a wide range of parameters, the USWI is in a meta-stable state and there exists the risk that the failure of a single line will lead to a large blackout, in which the yield falls below 0.8. As tolerance increases beyond 2.0, the risk of a large blackout decreases almost to 0.

We also showed that the level of line protection, p, increases the robustness of the grid, but to a lower extent than does the tolerance. An important parameter defining the robustness of the grid is the significance of the initial failure u. Given a particular α, when u is small, there is practically no risk of a large blackout, while when u approaches 1, the risk is maximal for a given α. If α is kept constant and u decreases, there is the same effect on the risk of a large blackout as when α increases and u is kept constant, meaning that the same effect could be achieved by protecting important lines as by increasing the overall tolerance.

Another important observation from our simulation is that upon failure of a line, the first few cascade time steps affect only the immediate vicinity of the failed line. During the first few time steps of the cascade, the yield does not significantly decrease, but it starts to drop quickly at the end of the latent period. The duration of the latent period of the cascade linearly increases with the line tolerances. Hence, increasing the line tolerances provides sufficient time for grid operators to intervene and stop the cascade.

Finally, we introduced the DADA model to generate synthetic power grids. We showed that the DADA model and the USWI have many common features. The physical features, such as the distribution of degrees, resistances, and currents, compare well in both models. The behavior of cascading failures in the DADA model is also similar to their behavior in the USWI power grid.

Overall, our results provide a useful understanding and insight of the general properties of cascading failures in power grids. Our findings can be used to increase the resilience of power grids against failures and to design optimal shedding and protection strategies for preventing cascades from spreading.

Acknowledgments

This work was supported in part by DTRA grants HDTRA1-10-1-0014, HDTRA1-14-1-0017, and HDTRA1-13-1-0021, U.S. DOE under Contract No. DE-AC36-08GO28308 with NREL, and funding from the U.S. DOE OE as part of the DOE Grid Modernization Initiative. We also acknowledge the partial support of this research through the Dr Bernard W. Gamson Computational Science Center at Yeshiva College. We thank Meric Uzunoglu and Andrey Bernstein for their help with processing the USWI data. We also thank Guifeng Su for his work on programming the preferential attachment algorithm and measuring "hop distance," Yehuda Stuchins for his preliminary work on studying relations between distance and failures, and Tzvi Bennoff for testing alternative parameters. We appreciate the assistance of Adam Edelstein, Jonathan Jaroslawicz, and Brandon Bier in sorting the data. We are grateful to S. Havlin, G. Paul, and H.E. Stanley for productive interactions. This work was done while Saleh Soltan was with Columbia University.

References

Albert, R., & Barabási, A.-L. (2002). Statistical mechanics of complex networks. *Reviews of Modern Physics*, **74**(1), 47–97.

Asztalos, A., Sreenivasan, S., Szymanski, B. K., & Korniss, G. (2014). Cascading failures in spatially-embedded random networks. *PloS one*, **9**(1), e84563.

Bakke, J. Ø. H., Hansen, A., & Kertész, J. (2006). Failures and avalanches in complex networks. *Europhysics Letters*, **76**(4), 717–723.

Bakshi, A. S., Velayutham, A., Srivastava, S. C., Agrawal, K. K., Nayak, R. N., Soonee, S. K., & Singh, B. (2012). Report of the enquiry committee on grid disturbance in Northern Region on 30th July 2012 and in Northern, Eastern & North-Eastern Region on 31st July 2012. New Delhi, India.

Barabási, A.-L., & Albert, R. (1999). Emergence of scaling in random networks. *Science*, **286**(5439), 509–512.

Bernstein, A., Bienstock, D., Hay, D., Uzunoglu, M., & Zussman, G. (2014). Power grid vulnerability to geographically correlated failures—analysis and control implications. In *Proceedings of the IEEE INFOCOM'14*, Toronto, Canada.

Bienstock, D. (2011). Optimal control of cascading power grid failures. In *Proceedings of the IEEE CDC-ECC'11*, Orlando, FL.

Bienstock, D., & Verma, A. (2010). The $N - k$ problem in power grids: New models, formulations, and numerical experiments. *SIAM Journal of Optimization* , **20**(5), 2352–2380.

Buldyrev, S. V., Parshani, R., Paul, G., Stanley, H. E., & Havlin, S. (2010). Catastrophic cascade of failures in interdependent networks. *Nature*, **464**(7291), 1025–1028.

Carreras, B. A., Lynch, V. E., Dobson, I., & Newman, D. E. (2002). Critical points and transitions in an electric power transmission model for cascading failure blackouts. *Chaos*, **12**(4), 985–994.

Carreras, B. A., Lynch, V. E., Dobson, I., & Newman, D. E. (2004). Complex dynamics of blackouts in power transmission systems. *Chaos*, **14**(3), 643–652.

Clauset, A., Shalizi, C. R., & Newman, M. E. J. (2009). Power-law distributions in empirical data. *SIAM Review*, **51**(4), 661–703.

Coniglio, A. (1981). Thermal phase transition of the dilute s-state potts and n-vector models at the percolation threshold. *Physical Review Letters*, **46**(4), 250.

De Arcangelis, L., Redner, S., & Herrmann, H. J. (1985). A random fuse model for breaking processes. *Journal de Physique Lettres*, **46**(13), 585–590.

Dobson, I., & Lu, L. (1992). Voltage collapse precipitated by the immediate change in stability when generator reactive power limits are encountered. *IEEE Transactions on Circuits Systems I, Fundamental Theory Application*, **39**(9), 762–766.

Glover, J. D., Sarma, M. S., & Overbye, T. (2012). *Power system analysis & design, si version*. Stamford, CT: Cengage Learning.

Hines, P., Balasubramaniam, K., & Sanchez, E. (2009). Cascading failures in power grids. *IEEE Potentials*, **28**(5), 24–30.

Kornbluth, Y., Barach, G., Tuchman, Y., Kadish, B., Cwilich, G., & Buldyrev, S. V. (2018). Network overload due to massive attacks. *Physical Review E*, **97**(5), 052309.

Manna, S. S., & Sen, P. (2002). Modulated scale-free network in euclidean space. *Physical Review E*, **66**(6), 066114.

Motter, A. E. (2004). Cascade control and defense in complex networks. *Physical Review Letters*, **93**(9), 098701.

Motter, A. E., & Lai, Y.-C. (2002). Cascade-based attacks on complex networks. *Physical Review E*, **66**(6), 065102.

Pahwa, S., Scoglio, C., & Scala, A. (2014). Abruptness of cascade failures in power grids. *Scientific Reports*, **4**, 3694.

Pinar, A., Meza, J., Donde, V., & Lesieutre, B. (2010). Optimization strategies for the vulnerability analysis of the electric power grid. *SIAM Journal on Optimization*, **20**(4), 1786–1810.

Platts. (2009). Electric transmission lines GIS data. Retrieved from `http://www.platts.com/Products/gisdata`.

https://doi.org/10.1017/nws.2018.14 Published online by Cambridge University Press

Soltan, S., Mazauric, D., & Zussman, G. (2014). Cascading failures in power grids: Analysis and algorithms. In *Proceedings of the ACM e-Energy'14*, Cambridge, UK.

US-Canada Power System Outage Task Force. (2004). Report on the August 14, 2003 blackout in the United States and Canada: Causes and recommendations. Retrieved from `https://reports.energy.gov`.

U.S FERC, DHS, & DOE. (2010). Detailed technical report on EMP and severe solar flare threats to the U.S. power grid.

Xulvi-Brunet, R., & Sokolov, I. M. (2002). Evolving networks with disadvantaged long-range connections. *Physical Review E*, **66**(2), 026118.

Zapperi, S., Ray, P., Stanley, H. E., & Vespignani, A. (1997). First-order transition in the breakdown of disordered media. *Physical Review Letters*, **78**(8), 1408–1411.

https://doi.org/10.1017/nws.2018.14 Published online by Cambridge University Press